Energy 36 (2011) 6583–6595

Contents lists available at SciVerse ScienceDirect

Energy

journal homepage: www.elsevier.com/locate/energy

Impact of injection conditions on flame characteristics from a parallel multi-jet burner

Jianchun Mi[a,b,*], Pengfei Li[b], Chuguang Zheng[c]

[a] State Key Laboratory of Turbulence & Complex Systems, Peking University, Beijing 100871, China
[b] Department of Energy & Resources Engineering, College of Engineering, Peking University, Beijing 100871, China
[c] State Key Laboratory of Coal Combustion, Huazhong University of Science and Technology, Wuhan 430074, China

ARTICLE INFO

Article history:
Received 17 March 2011
Received in revised form
30 August 2011
Accepted 2 September 2011
Available online 29 September 2011

Keywords:
Injection condition
Flameless combustion
MILD combustion
High temperature air combustion

ABSTRACT

This numerical study systematically investigates the influence of initial injection conditions of reactants on flame characteristics from a parallel multi-jet burner in a laboratory-scale furnace. In particular, varying characteristics from visible flame to invisible Moderate or Intense Low-oxygen Dilution (MILD) combustion is explored. Different parameters examined include the initial separation of fuel and air streams (S), air nozzle diameter (D_a), fuel nozzle diameter (D_f), and air preheat temperature (T_a). The present simulations agree qualitatively well with previous measurements reported elsewhere for two reference cases investigated by experiment. A number of new and significant findings are then deduced from the simulations. For instance, all S, D_a and D_f are found to play significant roles in achieving a proper confluence location of air and fuel jets for establishing the MILD combustion. Particularly, varying D_a is most effective for controlling the combustion characteristics. It is also found that the stability limits of the non-premixed MILD combustion varies with different combustor systems and inlet reactant properties. Moreover, for the first time, several analytical approximations are obtained that relate the flue-gas recirculation rate and the fuel-jet penetration to D_a, D_f, S and also reactant properties.

1. Introduction

The method of MILD (moderate or intense low-oxygen dilution) combustion has been recognized as one of the most successful combustion technologies, developed in past two decades, which can save energy and simultaneously reduce emissions of NO_x (nitric oxide) in particular. This technology, sometimes also termed as 'HiTAC or HTAC' (high temperature air combustion) [1], 'FLOX' ('flameless combustion' or 'flameless oxidation') [2], has been rapidly transferred from laboratory tests to industrial applications, in particular, for steel reheating and steel heat treatment furnaces. It has played a significant role in the mitigation of combustion-generated pollutants (particularly NO_x) and also of greenhouse gases by achieving high thermal efficiency in metallic industry. There is no reason that the technology is just limited within the above industry field; instead, it has an exceptionally great potential to benefit other industries in future.

The MILD combustion occurs volumetrically and is controlled by strong flue-gas recirculation. More specifically, fuel is slowly oxidized in an environment where oxygen is highly diluted by recirculated exhaust gases while temperature is beyond the local auto-ignition point of fuel. Under such conditions, traditional flames cannot sustain and are always blown-off due to either high jet velocity or strong internal flue-gas recirculation. Chemical reactions occur in a distributed zone with significantly reduced peak temperatures [2,3]. As a consequence, the flame is hardly visible, the temperature distribution is rather uniform, the net radiation flux increases by as much as 30%, and NO_x emissions reduce dramatically [1–3].

The MILD combustion has been a favourite subject of R&D (research and development) in the last two decades, see, e.g., [4–7]. Weber et al. [4,5] performed a series of experiments on the MILD combustion of gaseous, liquid and solid fuels. Their measurements were conducted inside a furnace operating with highly preheated air regime (1300 °C). Their data for NG (natural gas) showed that a substantial improvement in net flux of the thermal radiation can be achieved under the MILD combustion. Both the mixing pattern and intensity have significant effects on the overall performance of the furnace firing with NG, specifically on the thermal efficiency part. The combustion process of light oil is very similar to that of

* Corresponding author. Department of Energy & Resources Engineering, College of Engineering, Peking University, Beijing 100871, China. Tel./fax: +86 10 62767074.
E-mail address: jcmi@coe.pku.edu.cn (J. Mi).

0360-5442/$ – see front matter © 2011 Elsevier Ltd. All rights reserved.
doi:10.1016/j.energy.2011.09.003

natural gas, with invisible flames. However, combustion of heavy fuel oil and coal is significantly different, and the flames are always visible in their tests. Weber et al. [5] pointed out that further research is still needed to optimise the burner designs for maximising the recirculation and mixing inside the furnace. Note that their test furnace of square cross-section is characterized by a burner with a central (vitiated) air nozzle and two small off-axis fuel injectors, and an exhaust outlet opposite to the burner inlets. Experimental investigations of the MILD combustion using this burner-furnace configuration have been performed also by other investigators, e.g., Rottier et al. [8,9].

Szegö et al. [7] tested a furnace of different configuration for MILD combustion. In their setup, the fuel is injected through four off-axis holes and the air enters through a central nozzle, while four exhaust ports are located in between. These investigators reported measurements of temperature and flue-gas composition from conventional and MILD combustions using NG and LPG (liquefied petroleum gas) as fuels. They, as well as Kumar et al. [10], found that air preheating is not required to achieve MILD combustion. Their investigation [7] on the stability and operational condition found that diluting the fuel with an inert gas helps achieve the MILD condition. This is because the dilution shifts the stoichiometric contour to the high scalar dissipation region which suppresses flame propagation and leads to a distributed reaction further downstream [11]. A certain threshold of the fuel-air momentum ratio G_f/G_a ($\approx$0.006 for their test system) was claimed to be necessary for the MILD combustion to occur. This momentum rate was considered to ensure the penetration of fuel jets to a region classified as the oxidation zone.

Mi et al. [12,13] used a different burner configuration at the furnace indicated above in Refs. [6,7] to investigate, both experimentally and numerically, the effects of the air-fuel injection momentum rate and premixing the two on the MILD combustion. A number of different patterns of partially and fully premixed reactants were found to work very well for MILD combustion. Their numerical study suggested that there is a critical momentum rate of the inlet fuel-air mixture below which the MILD combustion does not occur. In the MILD regime, both the inlet fuel-air mixedness and momentum rate impose insignificant influence on exhaust emissions of the MILD combustion. It is worth noting that their fuel and air jets issued respectively from a central and an annulus nozzle (non-premixed) or both from an annulus nozzle (premixed). Later, Li et al. [14,15] further investigated impacts of various particular injection conditions on the characteristics of fully premixed MILD combustion from a single jet burner in the same furnace. The injection conditions include the area of the nozzle, equivalence ratio, thermal input, and initial dilution of reactants. They found that all these parameters have significant influence on the MILD combustion. It was also revealed that the premixed combustion can occur only when the injection Reynolds number exceeds its critical value. Moreover, very low emissions of NO_x, CO and H_2 were measured for the premixed MILD combustion under various conditions.

Very recently, Schaffel-Mancini et al. [16] have developed several concepts of the power station boiler firing pulverized-coal in the context of the three key points of MILD combustion: existence of an intensive in-furnace recirculation, homogeneity of both the temperature and the chemical species fields, and uniformity of heat fluxes. In order to determine the boiler shape and its dimensions, these authors performed CFD-based numerical simulations to optimise both the distance between burners and location of the burner block. It was demonstrated that the momentum of the combustion air stream is an essential design parameter driving the in-furnace recirculation. Also, the impact of the combustion air temperature on boiler performance was found less critical providing that the intensive in-furnace recirculation has been created. Schaffel-Mancini et al. [16] finally concluded that MILD technology could be a realizable, efficient and clean technology for pulverized coal fired boilers.

In the context of the previous work indicated above, the present study has been undertaken to systematically investigate the influence of injection conditions of separate methane and air streams on the establishment of diffusion MILD combustion in a furnace similar to that of Refs. [4,5,8]. The investigation is performed through RANS (Reynolds-averaged Navier–Stokes equations) modelling. Several injection conditions are selected that include the air preheat temperature (T_a), separation distance between fuel and air exits (S), air nozzle diameter (D_a) and fuel nozzle diameter (D_f). The main objective of the study is threefold:

(1) To qualitatively verify our simulations for MILD combustion by RANS-modelling with previous measurements of Rottier et al. [8,9];
(2) To explore whether the geometric parameters S, D_a and D_f or the initial properties of reactants are important for the occurrence of MILD combustion; and
(3) To identify the key factor(s) that determine the MILD combustion.

2. Computation details

2.1. Furnace configuration and reference cases for MILD combustion

The present study simulates various combustion cases occurring in a laboratory-scale furnace, some of which have been tested experimentally in a previous study of Rottier et al. [8,9]. The detail of the furnace is given in Refs. [8,9] and here only a brief description is provided on it. Fig. 1 shows a schematic of the furnace. The combustion chamber is square in cross-section of 500 mm by

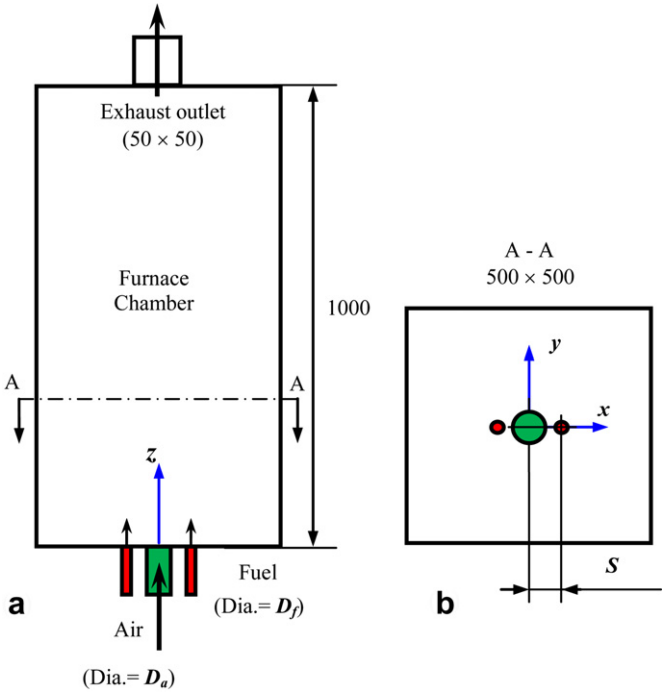

Fig. 1. Schematic of the furnace and burner configuration, simulated presently and measured previously in Rottier et al. [8]. (a) furnace and burner configuration; (b) nozzle arrangement. Dimensions are in mm.

500 mm and 1000 mm high, made with refractory materials for a maximum wall temperature of 1400 K. Several openings are set along in staggered rows on the four sides of the combustion chamber. These openings can receive an optical window or a probe stand for detailed measurements in the furnace, or a refractory block to preserve thermal confinement and measure wall temperature. The burner consists of a central air nozzle ($D_a = 25$ mm) and two off-axis fuel pipes ($D_f = 3$ mm), with the initial air-fuel separation $S = 50.7$ mm. The exhaust outlet (centreed) on the furnace top is square in cross-section with dimensions of 50 mm × 50 mm, according to Masson [17]. Combustion air can be preheated up to $T_a = 838$ K by an electric heater. The reference case for Rottier et al. [8] is the one under the operation conditions of firing methane (CH_4) at a thermal input of $P = 18.5$ kW, an equivalence ratio of $\phi = 0.85$ and an air preheat temperature of $T_a = 838$ K. They conducted a set of measurements by decreasing the preheat temperature from 838 K to 293 K when keeping constant other parameters. For those tests, the total mass flow rates of air and methane can be estimated to be $\dot{m}_a \approx 7.5 \times 10^{-3}$ kg/s and $\dot{m}_f \approx 3.7 \times 10^{-4}$ kg/s. Rottier et al. [8] reported that, for their reference case ($T_a = 838$ K), the wall temperature was homogeneous and equal to 1320 K, and the flame was invisible, so in the MILD combustion regime. They also stated that the MILD combustion applies for all their test cases.

For the present study, the above cases of $T_a = 838$ K and 293 K are set as reference cases to verify the RANS modelling.

2.2. Injection conditions of air and fuel for simulations

The present study is aimed at investigating the correlation of MILD combustion with the distance between the reactant exits (S), air preheat temperature (T_a), air nozzle diameter (D_a), and fuel nozzle diameter (D_f). Table 1 lists all the cases of present investigation. Note that numerical tests are performed for varying T_a, D_a, D_f or S in the first column at the listed values when keeping constant those parameters in the second column of the table.

2.3. Computational conditions and models

The commercial computational software package Fluent 6.3 [18] is used. Full three-dimensional structured grids are constructed to have small orthogonality deviations. The final grids for half model of all the cases listed in Table 1 are determined to be about 400,000–600,000 cells after checking the independence of simulated results on the grid number for the reference case; note that geometrical symmetry is used to reduce the computational time.

Fuel, air and flue gases are all assumed to obey the ideal gas law. Their specific heats are a function of temperature (piecewise-polynomial) [18]. Inlet and outlet boundary conditions of the computational domain for each case are set as constant velocities (corresponding to fuel and air injections), whose magnitude may vary when changing T_a, D_a and D_f, and constant static pressure (1.0 atm). Moreover, a uniform temperature distribution is set as the boundary condition of the entire inner wall of the furnace. The uniform temperature taken is justified because the wall temperature measured was indeed homogeneous [8]. For the reference case, the wall temperature of 1320 K, reported in Ref. [8], is employed for the calculation.

Table 1
Injection Conditions of Air and fuel for $P = 18.5$ kW and $\phi = 0.85$.

Injection conditions varied	Injection conditions fixed
T_a (K) = **293**[a], 423, 573, **838**[a]	$D_f = 3$ mm, $D_a = 25$ mm, $S = 50.7$ mm
D_a (mm) = 10, 15, 20, 25, 60, 80	$D_f = 3$ mm, $S = 50.7$ mm, $T_a = 838$ K
D_f (mm) = 2, 3, 5, 7, 9	$D_a = 25$ mm, $S = 100$ mm, $T_a = 838$ K
S (mm) = 20, 50, 100, 200	$D_f = 5$ mm, $D_a = 20$ mm, $T_a = 838$ K

[a] These cases are referred to as reference cases for the present study.

The standard k–ε model with the standard wall function is used for modelling the turbulent flow. The EDC (eddy dissipation concept) model with two-step chemical kinetic mechanisms for CH_4 and one-step mechanisms for C_2H_6 are applied. A preliminary study, aimed at checking the suitability of the global chemical kinetic mechanism for the simulation, is carried out by comparing the differences of the temperature distributions between a 2-D model with the global chemical kinetic mechanisms and a 2-D model with a detailed GRI-3.0 mechanism. (Similar checks were also performed in our previous studies [14,15].) The 2-D model is represented as the central cross-section of the furnace ($y = 0$, xz-plane). It is found that the result for mean temperature of the global mechanism model is similar to that obtained by the detailed GRI-3.0 mechanism, e.g., with the maximum difference between the predicted temperatures being about 20 K. For this reason, the global mechanisms (two-step chemical kinetic mechanisms for CH_4 and one-step mechanisms for C_2H_6) are used for all the present simulations in order to reduce the computational time and make simulations with 3-D furnace affordable. To lessen the computational cost of time integration, the present modelling adopts the in-situ adaptive tabulation (ISAT) model of Pope [19].

To model the gas emissivity, the DO (discrete ordinate) radiation model with WSGGM (weighted sum of gray gas model) is applied for radiation [20]. For DO radiation model, theta divisions and phi divisions define the number of control angles used to discretize each octant of the angular space, and the both parameters are set to 5. Theta Pixels and Phi Pixels are used to control the pixelation that accounts for any control volume overhang, and both parameters are set to 2. The SIMPLE algorithm is used for pressure velocity coupling. Moreover, the NO_x is computed by taking equilibrium conditions for the reaction $O_2 \leftrightarrow 2O$, see Ref. [21]. The NO_x formation rate is given by

$$\mathrm{d[NO]}/\mathrm{d}t = 2k_{\mathrm{Nlf}}[\mathrm{O}]_{\mathrm{eq}}[\mathrm{N_2}],$$

where $k_{\mathrm{Nlf}} = 1.8 \times 10^{11} \exp[-38370/T]$ m^3/kmols.

A second-order discretization scheme is used to solve all governing equations. Convergence is obtained when the residuals are less than 10^{-6} for energy and DO intensity and 10^{-5} for all other variables. The outlet temperature and velocity are monitored and their variations within 1 K and 0.1 m/s, respectively, are allowed for convergence of the solution. Simulations are performed with a 16-core CPU and 26 GB memory workstation (HP-Z800).

3. Definitions of fuel-jet penetration and relative recirculation rate

3.1. Fuel-jet penetration (Z_J)

For the non-premixed or diffusion combustion, fuel and oxidant streams must discharge individually into furnace from their own nozzles, flow downstream separately over some distance prior to their confluence, and then merge as a single jet, see Fig. 2. The fuel-jet penetration, denoted by Z_J, is defined as the vertical distance from the fuel-nozzle exit to the location at which the (weak) fuel jet has just attached to the (strong) air jet. In the present paper, Z_J is estimated to be the minimum value of z at which only one peak occurs at the centreline in the mean velocity (v_z) profile across the xy plane.

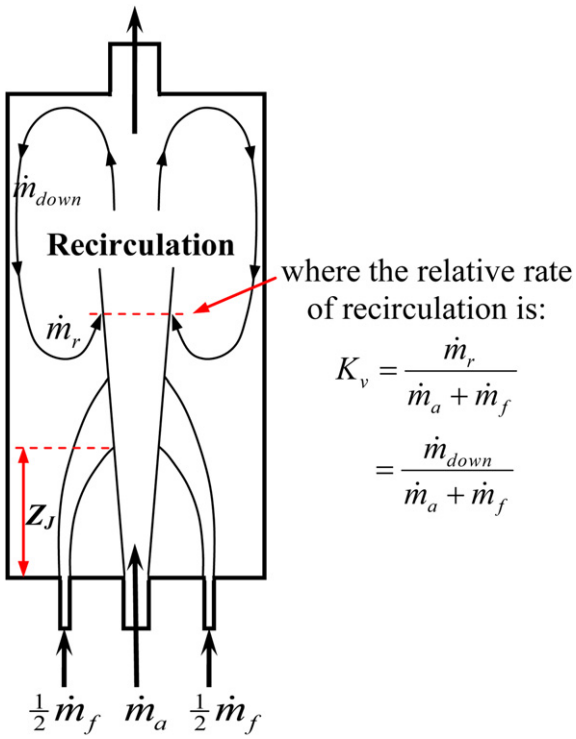

Fig. 2. Definitions of the fuel-jet penetration and relative rate of the exhaust-gas recirculation.

3.2. Relative recirculation rate (K_v)

The intense dilution of reactants prior to their global combustion reactions is one of the vital requirements for achieving overall MILD combustion in the downstream region at $z \geq Z_J$. The degree of low-oxygen dilution may be measured by the relative entrainment rate of the exhaust gas into the reactant stream(s), first defined by Wünning & Wünning [2] as the recirculation rate (using this term throughout the paper for consistency), viz.,

$$K_v = \dot{m}_r / \left(\dot{m}_a + \dot{m}_f\right), \tag{1}$$

where $\dot{m}_r$ is the mass flux of the exhaust gas recirculated and then entrained while $(\dot{m}_a + \dot{m}_f)$ denote the total mass flow rate of the injecting reactants (i.e., air and fuel). For the present cases, according to the mass conservation law, at each cross section of the chamber, the mass flux of the exhaust gas entrained, $\dot{m}_r$, must equal to the downward mass flux of the recirculated exhaust gas, $\dot{m}_{\mathrm{down}}$, namely

$$\dot{m}_r(z) = \dot{m}_{\mathrm{down}}(z) = \int\!\!\int_{A(z)} \rho v_z(x,y)\mathrm{d}x\mathrm{d}y \tag{2}$$

with $A(z)$ being the area for $v_z < 0$. For the same flux of reactants, a higher value of $\dot{m}_{\mathrm{down}}$ reflects a higher entrainment rate of the exhaust gas and thus a greater recirculation rate or a higher value of K_v. It is worth noting that a greater value of K_v or $\dot{m}_r$ corresponds to a lower value of the local averaged oxygen concentration, C_{O_2}, and thus a higher degree of low-oxygen dilution, since $C_{O_2} \approx \dot{m}_{O_2}/(\dot{m}_{O_2} + \dot{m}_{N_2} + \dot{m}_f + \dot{m}_r)$ and $\dot{m}_a \approx \dot{m}_{O_2} + \dot{m}_{N_2}$.

Here a note should be taken on the dependence on Z_J of $K_v(z = Z_J)$ or simply $K_v(Z_J)$. As defined, separate fuel and air streams globally meet and mix each other at $z \geq Z_J$. In the region upstream from this location, both fuel and oxidant are gradually diluted by the recirculation and entrainment of hot combustion products into their individual streams. Whether or not the MILD combustion can be established depends on the degree of this dilution. Apparently, as Z_J increases, $K_v(Z_J)$ becomes greater and so occurs a higher dilution that enhances the occurrence of MILD combustion.

4. Results and discussion

4.1. Present predictions versus previous measurements for the reference cases

Rottier et al. [8] found that the MILD combustion mode occurs for the case with $T_a = 838$ K and also that when reducing the combustion air to a temperature of $T_a = 293$ K. To check the validity of the RANS modelling, the present predictions are compared with their measurements in Fig. 3(a) and (b). These two figures show the predicted distributions of the mean temperature (T) in the central xz plane ($y = 0$) and those of the measurements [8] for $T_a = 838$ K and 293 K, respectively. Rottier et al. [8] used a thermocouple of 50-μm bare B-type to measure the mean temperatures point by point at numerous locations through several windows. So, they could not provide a set of perfect measurement data since their point-measurements were made obviously at different times over a certain period in which the whole operation was impossible to keep at an invariable state; besides, the limited number of measured locations should be another negative factor for plotting temperature contours. It is hence understood that their resulting temperature maps are quite scattering and definitely with significant errors. Also, it is unfortunate that they did not provide any XY-plots of their measured data, so that we cannot make better quantitative comparisons for the mean temperature. Nevertheless, taking into consideration all the factors that influence the measurement accuracy, a careful check of the images suggests that the calculated and measured results of the mean temperature qualitatively agree reasonably well for both cases with $T_a = 838$ K and 293 K.

Specific observations then should be made here from Fig. 3(a) and (b). As two small fuel jets proceed downstream, they are tending to the central air jet and simultaneously mixing the surrounding flue gas where the oxygen concentration $[O_2] \approx 4\%$. In the low-oxygen and fuel-rich mixing layer, oxidation takes place slowly, with a small amount of heat releasing, and thus temperature rises slightly (reflected by a thin yellow or faint-red layer in Fig. 3(a) or (b)). The slow oxidation consumes almost all the oxygen so that $[O_2] \approx 0$ in the mixing layer of the fuel jet (see Fig. 6 below). Before their confluence ($z < Z_J$), the main fuel and air jets all have entrained a large quantity of hot combustion products and hence been well diluted (and heated up) through their mixing layers. When they globally mix each other at $z \geq Z_J$, no fast oxidation is possible and, instead, slow reactions take place volumetrically, therefore no flame front being formed. Under such circumstances, the overall MILD combustion is established, regardless of $T_a = 293$ K or 838 K. This was confirmed experimentally by Rottier et al. [8], who showed that the flame front is invisible across the entire chamber and therefore the combustion is certainly in the flameless MILD mode for the two cases. Nevertheless, both the calculations and the measurements (see Fig. 3a,b) consistently reveal that preheating the combustion air from $T_a = 293$ K to $T_a = 838$ K not only shifts the central main reaction zone towards the burner exit but also reduces the volume of the reaction zone. Besides, the maximum temperature in the main reaction zone is about 200 K (400 K) higher than the mean temperature of the recirculated exhaust gas for $T_a = 293$ K (838 K).

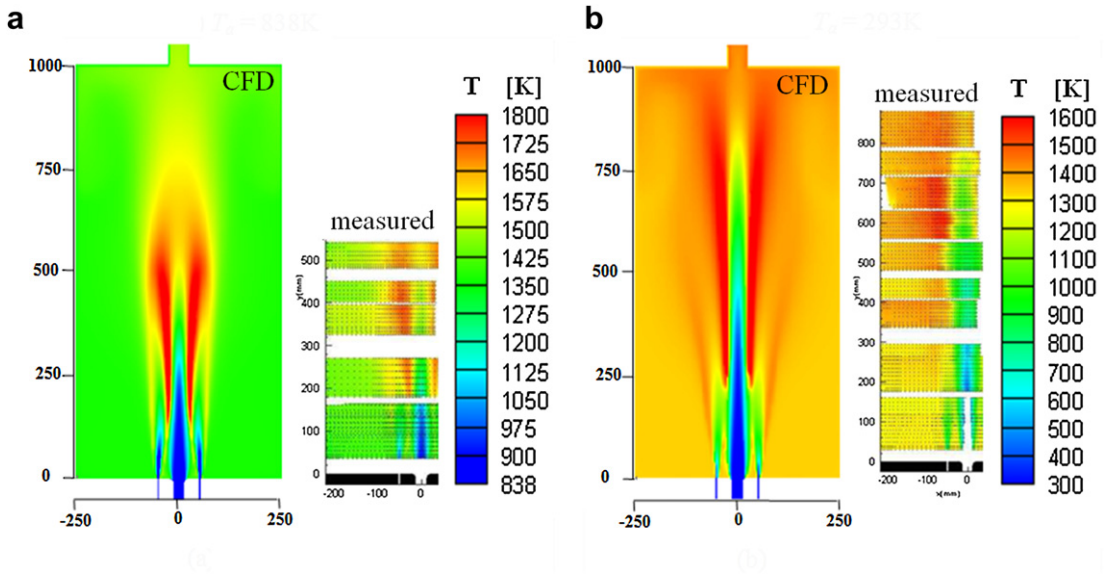

Fig. 3. Present predictions versus previous measurements [8] of the mean temperature in the central *xz* plane for the reference cases: $D_f = 3$ mm, $D_a = 25$ mm, $S = 50.7$ mm, $P = 18.5$ kW and $\phi = 0.85$. Air preheat temperature: (a) $T_a = 838$ K; (b) $T_a = 293$ K. Note that the two images of the measured data [8] were reproduced directly from the original paper [8] and thus that the two contour scales used in [8] for $T_a = 838$ K and 293 K are also selected for presenting the present data. Dimensions are in mm.

4.2. Dependence of the diffusion combustion on injection parameters

4.2.1. Effect of varying the preheat temperature of combustion air (T_a)

To investigate the effect of T_a, Fig. 4(a)–(d) display contours of the calculated mean temperature (T) in the central *xz* plane ($y = 0$), while Fig. 5(a)–(d) shows those of the calculated O_2 concentration, for T_a varying from 293 K to 838 K. As T_a is increased, chemical reaction between fuel and 'warmer' air should become faster so that the central main reaction zone at $z > Z_J$ shifts upstream (towards the burner) and also decreases in size. In other words, an increase in T_a should cause the high temperature (>1500 K) zone (yellow to red colors) moving closer to the burner while the maximum temperature should increase and occur upstream —– as is indeed seen in Fig. 4 (and also Fig. 3). This is also reflected by the

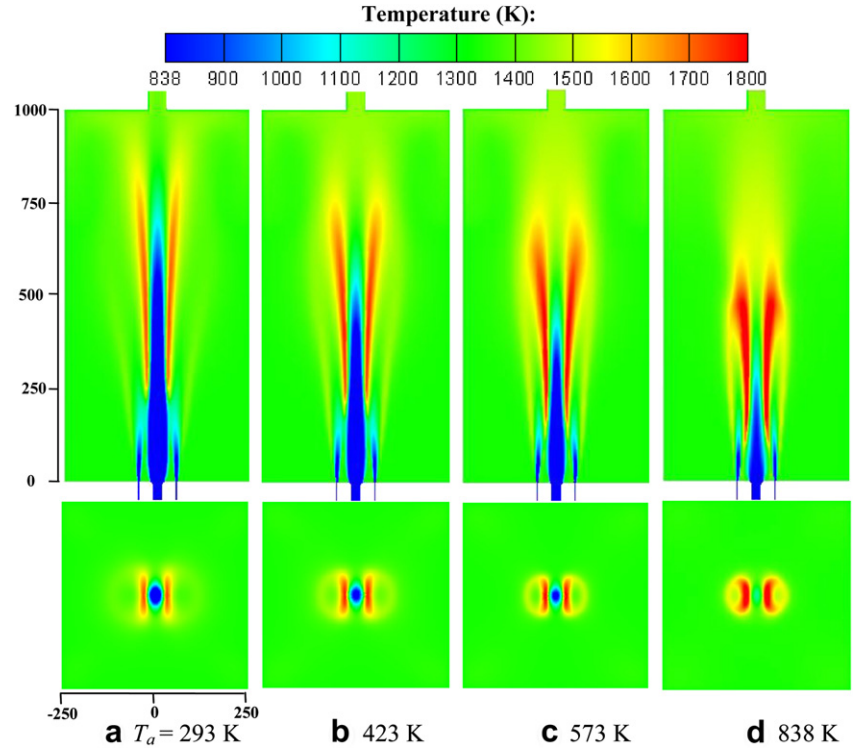

Fig. 4. Effect of air preheat temperature T_a on mean temperature distributions in the central *xz* plane (upper) and the *xy* plane where T_{max} occurs (lower) for the reference case: $D_f = 3$ mm, $D_a = 25$ mm, $S = 50.7$ mm, $P = 18.5$ kW and $\phi = 0.85$. Dimensions are in mm.

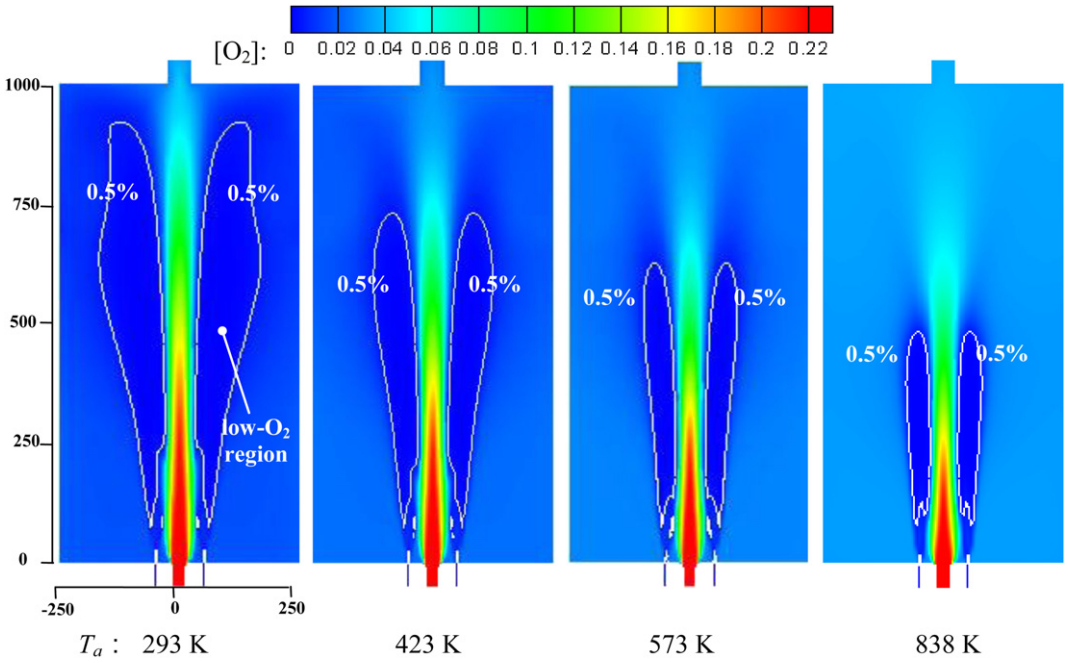

Fig. 5. Contours of the O_2 concentration in the central xz plane ($y = 0$) at different preheat temperatures for $D_f = 3$ mm, $D_a = 25$ mm, $S = 50.7$ mm, $P = 18.5$ kW and $\phi = 0.85$. Dimensions are in mm.

region of near-zero oxygen concentration (a blue zone surrounded by the contour of $[O_2] = 0.5\%$) shown in Fig. 5. These observations agree qualitatively well with the measured results of Rottier et al. [8] for both the mean temperature (see Fig. 3) and the mean OH concentration (see their Fig. 5). Their Fig. 5 shows that, as T_a is increased, the concentration of OH increases while the high OH region moves upstream; correspondingly, the local heat release rate grows and the main reaction zone shifts towards the burner exit.

4.2.2. Effect of varying the air nozzle diameter (D_a)

Figs. 6–9 respectively display contours of the mean temperature (T), O_2 (left)/CH_4 (right) concentrations, CO_2 (left)/CO (right) concentrations and NO_x concentrations in the central xz plane ($y = 0$) obtained for D_a varying from 10 mm to 80 mm. Evidently, as D_a is decreased from 25 mm (reference case) to 10 mm, the CO_2 and CO concentration gradients in the reaction zone reduce significantly, particularly the mean temperature becomes extremely uniform and no high-temperature region at all appears to exist across the furnace, thus reflecting better performances of the MILD combustion; note that the combustion for $D_a = 25$ mm is in the MILD regime based on the experimental result [8]. However, the situation is totally different when D_a is increased from 25 mm to 60 mm and 80 mm: the fast oxidation process and thus high heat release or high mean temperature occur in a significantly narrower zone. For these cases, the maximum mean temperature T_{max} reaches as high as 1974 K and 2142 K respectively, and so the traditional combustion with visible flames is expected to occur. Interestingly, Fig. 8 shows that the high CO region ($\geq$1.0%) grows considerably as D_a is increased from 25 mm to 80 mm.

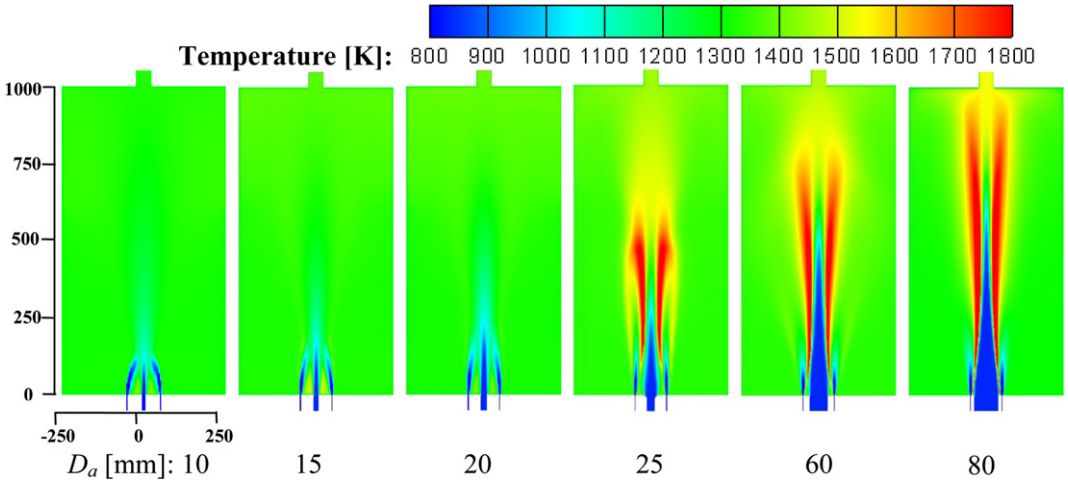

Fig. 6. Effect of the air nozzle diameter on mean temperature distributions in the central xz plane for $D_f = 3$ mm, $S = 50.7$ mm, $T_a = 838$ K, $P = 18.5$ kW and $\phi = 0.85$. Dimensions are in mm.

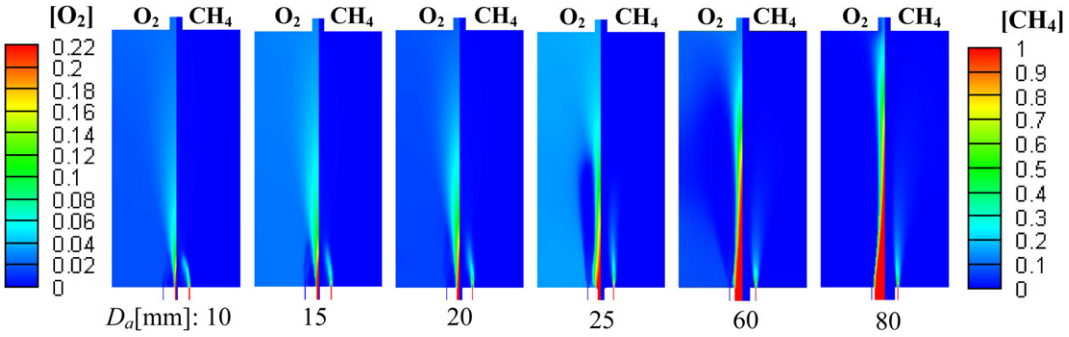

Fig. 7. Effect of the air nozzle diameter on O_2 and CH_4 concentration distributions in the central *xz* plane for $D_f = 3$ mm, $S = 50.7$ mm, $T_a = 838$ K, $P = 18.5$ kW and $\phi = 0.85$.

By comparison, the CO concentration is nearly uniform at [CO] ≈ 0.3%–0.4% across the furnace for $D_a < 25$ mm. Also, as demonstrated in Fig. 9, the NO_x formation is nearly zero across the entire furnace for $D_a < 25$ mm and very significant in the high-*T* regions for $D_a = 60$ mm and 80 mm; particularly interestingly, the exhaust emission of NO_x for the traditional combustion with $D_a = 80$ mm is about 300 times that for the MILD combustion even with $D_a = 25$ mm (not $D_a \leq 20$ mm).

Moreover, a careful inspection to Fig. 6 finds that the exhaust temperature at the furnace outlet, T_{out}, takes the highest value for $D_a = 80$ mm and successively lower for $D_a = 60$ mm, 25 mm and 20 mm. For $D_a \leq 20$ mm, T_{out} is nearly invariable. This variation results perhaps from a decreased rate of heat transfer, out of the chamber, caused by slower recirculation of the exhaust gas due to increasing D_a. In addition, the present calculations find higher emissions of the exhaust O_2 and CO for $D_a \geq 25$ mm than for $D_a < 25$ mm, suggesting that the conventional combustion may be less efficient than the MILD combustion.

The above observations may be explained as follows. In general, for the same mass flux of the central air jet ($\dot{m}_a$), as D_a is increased, the air jet injection momentum rate G_a decreases (cf. Eq. (3) in Section 5) and consequently the air jet entrainment (then the recirculation of exhaust gases) reduces (which will be quantified later). This obviously does not benefit for the establishment of MILD combustion. There is another negative effect of increasing D_a: namely, it reduces the effective separation of the fuel and air jets, i.e., $S_e = S - (D_a + D_f)/2$, and thus beneficial for the traditional combustion to occur. On the other hand, an increase in D_a makes the fuel jets to become relatively 'stronger' and thus to penetrate more deeply, see Figs. 6–9. However, as quantified later by the recirculation rate (K_v), the first negative effect of increasing D_a is much stronger than the positive one, so that an increase in D_a actually results in a great decrease in oxygen dilution by the exhaust gas recirculated prior to the confluence of the diluted fuel and oxygen at $z = Z_J$, thus accelerating the reaction rate between CH_4 and O_2.

4.2.3. Effect of varying the fuel nozzle diameter (D_f)

Figs. 10 and 11 demonstrate the effect of varying D_f on the mean temperature/oxygen concentration and the CH_4/CO_2 concentrations in the central *xz* plane for the cases with $D_a = 25$ mm and $S = 100$ mm. Here the distance between the air and fuel jet nozzle centres is selected to be $S = 100$ mm and D_f is varied from 2 mm to 9 mm so as to reduce the cross influence of varying D_f and also the effective separation of the fuel and air jets, i.e., $S_e = S - (D_a + D_f)/2$; apparently the cross influence decreases with increasing S and decreasing D_a or D_f. As D_f is increased, the fuel momentum rate G_f decreases (see Eq. (3) in Section 5), the fuel jets weaken, thus their penetration Z_J reduces (indeed evident in Fig. 10(a–e)) and, accordingly, both the fuel and air jets are less diluted by the entrained flue gas. In other words, an increase in D_f makes both the O_2 and CH_4 concentrations to become locally higher so that CH_4 is locally oxidized more rapidly in the region upstream of Z_J. Concurrently, the maximum temperature T_{max} due to combustion grows and thus the mean temperature distribution becomes less uniform. Figs. 10 and 11 also demonstrate that the reaction zone decreases in size and shifts upstream as D_f is increased. Apparently from Figs. 4 and 5 and Figs. 10 and 11, the effect of increasing D_f is roughly similar to that of increasing T_a; namely, both drive the combustion to depart from the MILD regime.

4.2.4. Effect of varying the separation of the fuel and air exits (S)

The initial separation (S) between the centres of the fuel and air jets should be another important factor that influences the MILD combustion characteristics. To check this, Fig. 12(a)–(c) present the mean temperature and oxygen concentration fields, while

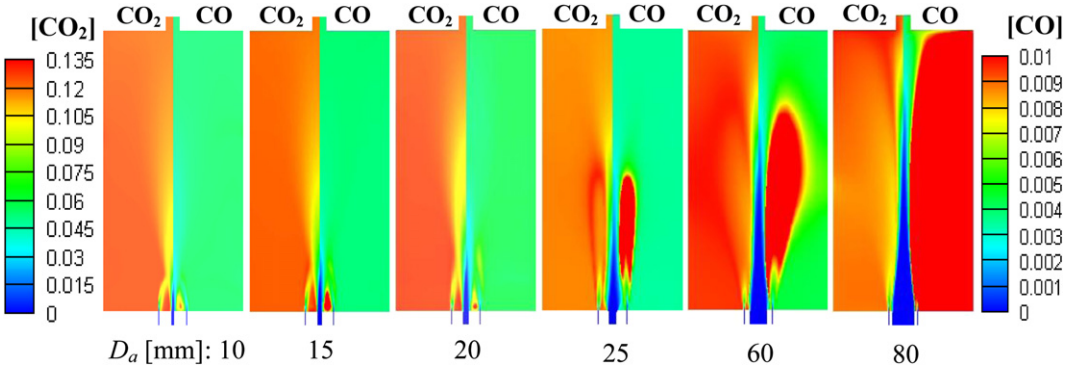

Fig. 8. Effect of the air nozzle diameter on CO_2 and CO concentration distributions in the central *xz* plane for $D_f = 3$ mm, $S = 50.7$ mm, $T_a = 838$ K, $P = 18.5$ kW and $\phi = 0.85$.

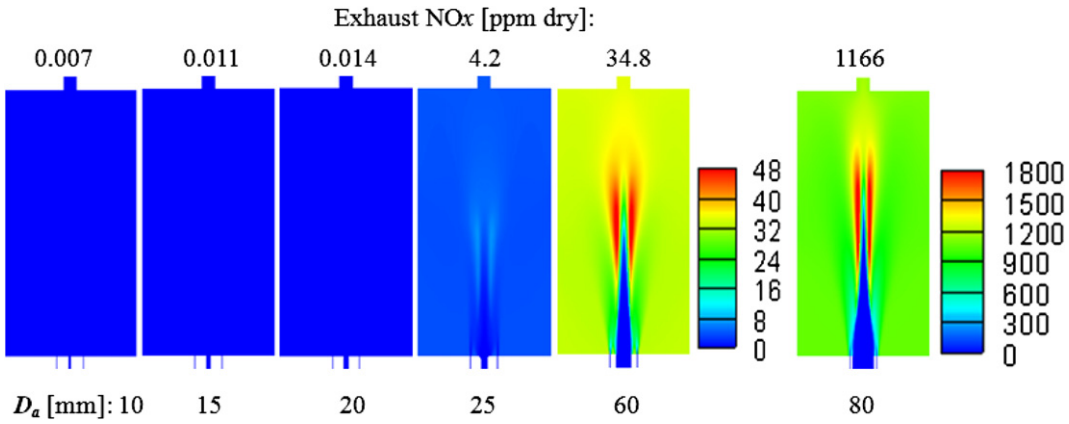

Fig. 9. Effect of the air nozzle diameter on NO_x concentration distributions in the central *xz* plane and on exhaust NO_x emissions for $D_f = 3$ mm, $S = 50.7$ mm, $T_a = 838$ K, $P = 18.5$ kW and $\phi = 0.85$.

Fig. 13(a)–(c) show the CH_4 and CO_2 concentrations, over the central *xz* plane for S [mm] = 50, 100 and 200. Obviously, the fuel jet penetration Z_J increases with increasing the separation S. It follows that increasing S causes both fuel and air jets to entrain more exhaust gases or to be diluted more thoroughly before their confluence at $z = Z_J$. Hence, as S is increased, not only the combustion reaction slows down but also the reaction zone grows in size, so that the temperature becomes more uniform and its maximum drops, see Figs. 12 and 13.

4.3. Effects of injection parameters on Z_J and $K_v(Z_J)$

Figs. 9–13 demonstrate that increasing D_f and S can make the fuel jet to penetrate more deeply, before its confluence with the central air jet, and accordingly the main reaction to occur in a lower-oxygen diluted zone. It is deduced that a sufficient increase in D_f or S and thus in the penetration distance Z_J may enable the combustion regime to transfer from the traditional to MILD mode. However, when examining the effect of D_a, see Figs. 6–8, the increase of Z_J does not appear to be always beneficial for the establishment of MILD combustion. It should be therefore significant to quantify the influences of the four injection parameters, i.e., D_a, D_f, S and T_a, on both Z_J and $K_v(Z_J)$.

Fig. 14(a–d) shows their effects on Z_J for $P = 18.5$ kW and $\phi = 0.85$. It is evident that Z_J basically increases as D_a or S increases but decreases with increasing D_f. Also, S seems to have the strongest influence on Z_J while D_a has the weakest. Note, nevertheless, that increasing D_a from 60 mm to 80 mm reduces the effective separation of the initial fuel and air jets, i.e., $S_e = S - (D_a + D_f)/2$, from 19.2 mm to 9.2 mm, thus reducing a reduction of Z_J, see Fig. 14(b), due to the opposite effects of D_a and S_e.

Since the relative rate of exhaust-gas recirculation, $K_v(Z_J)$, undoubtedly depends on Z_J, it thus must be a function of D_a, D_f and S. This is indeed confirmed in Fig. 15. As demonstrated, $K_v(Z_J)$ decreases significantly with increasing D_f and especially D_a but increases with enlarging S. Apparently, the effect of varying D_a on $K_v(Z_J)$ and thus on dilution of reactants is strongest, noting that $K_v(Z_J)$ for $D_a = 10$ mm is about 14 times that for $D_a = 80$ mm. In other words, varying D_a from 10 mm to 80 mm (even to 25 mm) change the combustion structure completely, see Fig. 6. Moreover, the effect of T_a on both Z_J and $K_v(Z_J)$ is found insignificant (Fig. 14(d)). This is consistent with the finding of Schaffel-Mancini et al. [16] that the impact of the combustion air temperature on the performance of coal-firing boiler is not critical if the intensive in-furnace recirculation has been created for MILD combustion.

Now let us examine the effects of Z_J on $K_v(Z_J)$ and T_{max}, the maximum mean temperature, which is also a key parameter in MILD combustion as it is responsible for NO_x production. The results obtained from variations of D_a, D_f and S are presented in Fig. 16. To make a meaningful comparison for different cases, normalization of Z_J by D_a is necessary since the initial momentum rate of the central air jet is much higher than that of the fuel jets and thus dominates the in-furnace flow structure. It is evident that, in general, as Z_J/D_a increases, $K_v(Z_J)$ increases whereas T_{max}

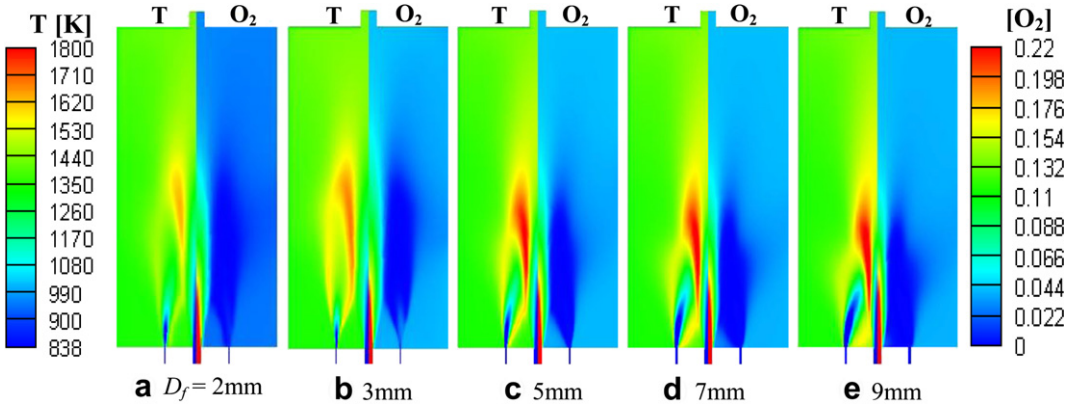

Fig. 10. Effect of the fuel nozzle diameter D_f on the mean temperature and O_2 concentration in the central *xz* plane for $D_a = 25$ mm, $S = 100$ mm, $T_a = 838$ K, $P = 18.5$ kW and $\phi = 0.85$.

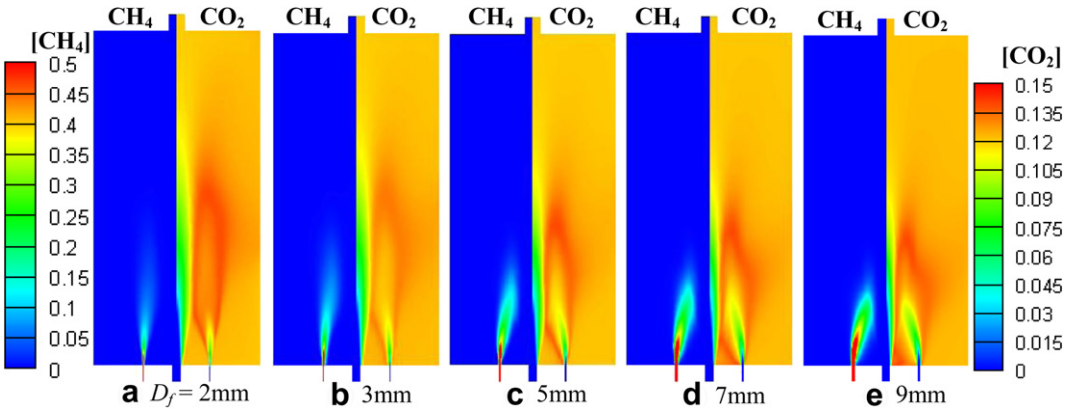

Fig. 11. Effect of the fuel nozzle diameter D_f on the CH_4 and CO_2 concentrations in the central xz plane for $D_a = 25$ mm, $S = 100$ mm, $T_a = 838$ K, $P = 18.5$ kW and $\phi = 0.85$.

decreases. Namely, the low value of T_{max} corresponds to high $K_v(Z_J)$ and *vice versa*. However, the three sets of data for either $K_v(Z_J)$ or T_{max} do not collapse onto a single curve. In particular, the data related to the D_a-variation behave quite differently when $D_a \leq 20$ mm. As D_a varies from 10 mm to 20 mm, T_{max} varies little (1410 K–1490 K) while $K_v(Z_J)$ changes significantly. Close looks at Figs. 6–10 suggest that the underlying in-furnace flow and combustion structures for these three cases differ substantially from the rest cases of varying D_a.

5. Further analysis and discussion

Figs. 3–13 demonstrate that the preheat temperature (T_a) and the geometric parameters (D_a, D_f, S) of air-fuel injections all have significant influence on the diffusion combustion characteristics. In particular, the most influential factor appears to be the air nozzle diameter (D_a). These results are further analyzed below.

The momentum flux (G_a) of the central air jet is much higher than (~200 times) that of each fuel jet (G_f) so that the air jet is expected to be only weakly affected by the fuel jets. These momentum fluxes can be expressed as

$$G_a = \frac{4\dot{m}_a^2}{\pi\rho_a D_a^2} \text{ and } G_f = \frac{4\dot{m}_f^2}{\pi\rho_f D_f^2}, \tag{3}$$

and then their ratio as

$$\frac{G_f}{G_a} = \frac{\rho_a}{\rho_f}\left(\frac{\dot{m}_f}{\dot{m}_a}\right)^2\left(\frac{D_a}{D_f}\right)^2 = \phi^2\gamma_s^{-2}\frac{T_f}{T_a}\left(\frac{D_a}{D_f}\right)^2, \tag{4}$$

where ρ_a and ρ_f are the initial air and fuel densities, γ_s is the stoichiometric air-fuel ratio ($\approx$17.11 for CH_4), and T_f is the initial fuel temperature. When the furnace is assumed to be sufficiently large, the central air jet may be ideally regarded as a single, free turbulent jet. The corresponding fuel jets are initially parallel to and eventually merge to the air jet at a certain downstream point (X_J, Z_J). That is, each fuel jet exhibits a curved trajectory, $X(z)$, towards the air jet and intercepts the mean boundary of the air jet at $z = Z_J$ (see Fig. 2).

We consider here a simplified case of single jet where the effect of buoyancy is negligible and the jet is statistically axisymmetrical. As proved well by previous independent investigations (e.g. [22,23]), the mean boundary of the jet can be described by the linear relation

$$B = C_s z \tag{5}$$

while the mass flow rate is

$$\dot{m} = C_e(z - z_o)\sqrt{0.25\pi\rho_\infty G_o}; \tag{6}$$

here C_s and C_e are experimental constants ($\approx$0.2 and 0.32 for a single free jet, see Ref. [23]), z_o is the z-location of the virtual origin, ρ_∞ is the flue-gas density, and G_o is the original jet

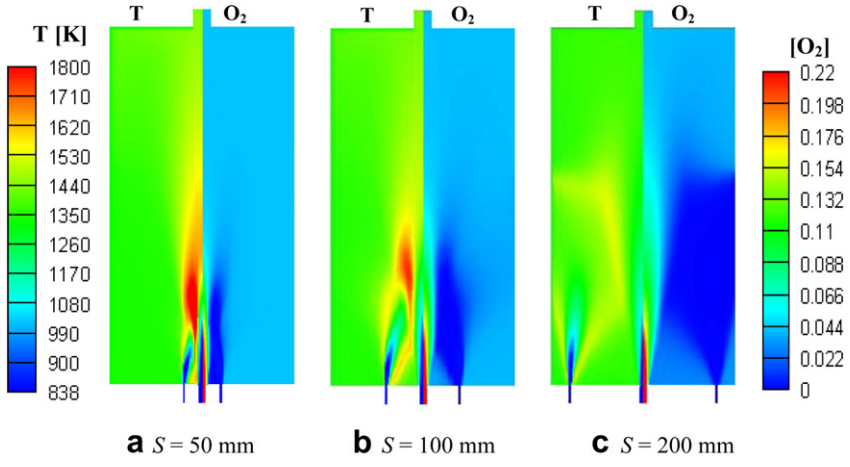

Fig. 12. Effect of S on the mean temperature field and O_2 concentration in the central xz plane for $D_f = 5$ mm, $D_a = 20$ mm, $T_a = 838$ K, $P = 18.5$ kW and $\phi = 0.85$.

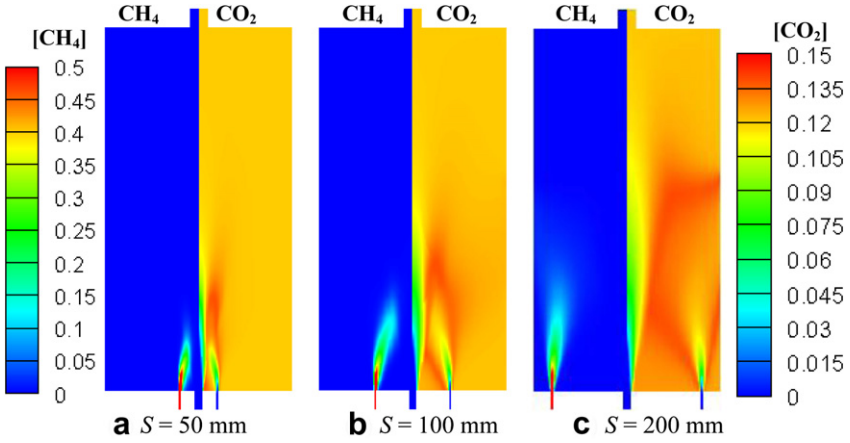

Fig. 13. Effect of S on the CH_4 and CO_2 concentrations in the central xz plane for $D_f = 5$ mm, $D_a = 20$ mm, $T_a = 838$ K, $P = 18.5$ kW and $\phi = 0.85$.

momentum flux. Accordingly, for the present study, the ratio of the mass entrainment rate ($\dot{m}_r = \dot{m} - \dot{m}_o$) of the surrounding gas at $z \geq Z_J$ to the original injection rate of reactants ($\dot{m}_o = \dot{m}_a + \dot{m}_f$), i.e., K_v defined in Eq. (1), may be estimated by

$$K_v = \frac{\dot{m}_r}{\dot{m}_o} \approx C_e \frac{(z - z_o)}{D_a} - 1. \tag{7}$$

To verify Eq. (7), Fig. 17 presents the K_v data against z/D_a over the region of 400 mm $\leq z \leq$ 800 mm for different D_a. Surprisingly, Eq. (7) works extremely well when taking $C_e \approx 0.2$, for the combustor system modelled, despite the virtual origin z_o varying with D_a. It is even roughly valid for $D_a > 25$ mm (when C_e is modified slightly), where the furnace should not be considered large enough for the present reactant jets to be 'free'.

In this context, we can specify the analysis of Grandmaison et al. [24] for the present system of parallel air jet/fuel jets and derive the following approximations for the fuel jet penetration Z_J and the recirculation rate $K_v(Z_J)$:

$$Z_J \approx C_1 \left(\frac{G_f}{G_a}\right)^{1/4} S \tag{8}$$

and

$$K_v(Z_J) \approx C_1 C_e \left(\frac{G_f}{G_a}\right)^{1/4} \frac{S}{D_a} + C_2, \tag{9}$$

where C_1 and $C_2[=-(C_e z_o/D_a+1)]$ are constants that should be determined by experiment or numerical simulation; their magnitudes should depend on combustion systems of investigation. Further, substitutions of Eq. (4) into Eqs. (8) and (9) attain that

$$Z_J \approx C_1 \phi^{-1/2} \gamma_s^{-1/2} \left(T_f/T_a\right)^{1/4} D_a^{1/2} D_f^{-1/2} S \tag{10}$$

$$K_v(Z_J) \approx C_1 C_e \phi^{-1/2} \gamma_s^{-1/2} \left(T_f/T_a\right)^{1/4} D_a^{-1/2} D_f^{-1/2} S + C_2. \tag{11}$$

Eqs. (8)–(11) can be checked by comparing them with simulated results for different geometric parameters D_a, D_f, and S. We test Eq. (8) in Fig. 18 using the data obtained under varying D_a and D_f. It is evident that this approximation, in general, works well with $C_1 \approx 4.9$ no matter whether the momentum ratio G_f/G_a is varied by changing D_a or D_f. There is an exception for $D_a = 80$ mm because too large a dimension of the air jet, confined in the furnace, has strongly violated the conditions for Eqs. (5) and (6). Since both Eqs. (7) and (8) hold quite well (see Figs. 17 and 18), Eq. (9) should be valid approximately as well.

In this context, it is deduced that Eqs. (10) and (11) should be applicable. Indeed, as seen in Fig. 14, Eq. (10) works fairly well for all the geometric parameters while Eq. (11) is good for S but not so for D_f and D_a, especially for the cases with $D_a = 60$ mm and 80 mm. In addition, Eq. (10) provides a correct trend for the T_a dependence of Z_J: i.e., Z_J increases with decreasing T_a, which is consistent with the modelling result.

As noted early, both K_v and Z_J are important parameters for the occurrence of diffusion MILD combustion. Increasing them yields a higher dilution of reactants by exhaust gases (e.g., CO_2, H_2O, N_2) and therefore beneficial for establishing the MILD combustion. It is thus useful for burner designers to find key factors of operation that control the magnitudes of K_v and Z_J. Eqs. (10) and (11) suggest that Z_J and K_v depend not only on burner geometric parameters (e.g., D_a, D_f, S) but also on the initial properties of reactants, i.e., fuel type,

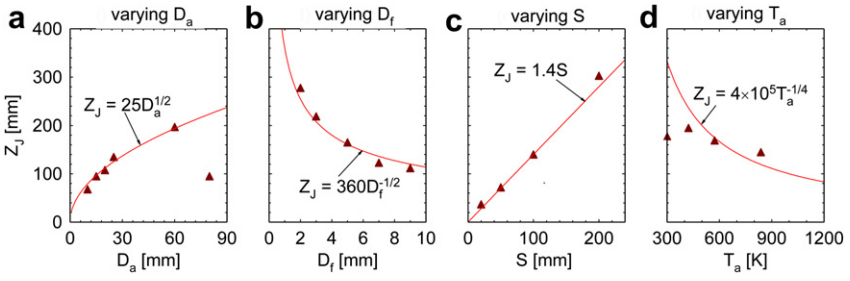

Fig. 14. Influences of D_a, D_f, S and T_a on Z_J for $P = 18.5$ kW and $\phi = 0.85$.

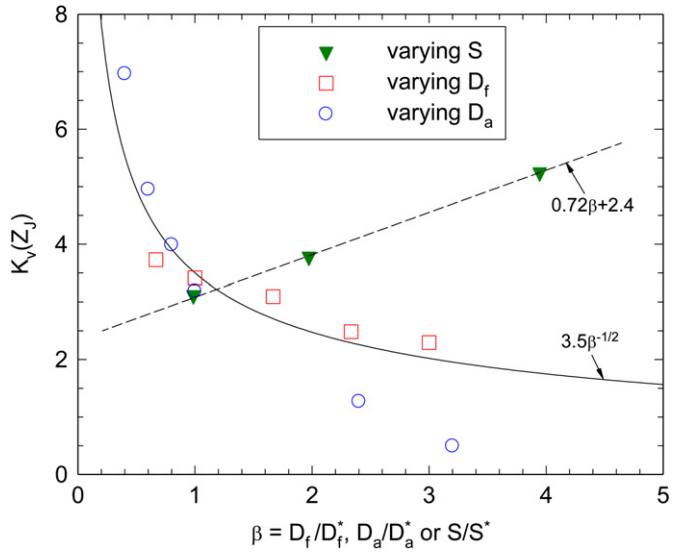

Fig. 15. Effects of D_a, D_f, and S on $K_v(Z_J)$ for $P = 18.5$ kW and $\phi = 0.85$. The abscissa is normalized by the reference quantity, i.e., $D_a^* = 25$ mm, $D_f^* = 3$ mm, or $S^* = 50.7$ mm.

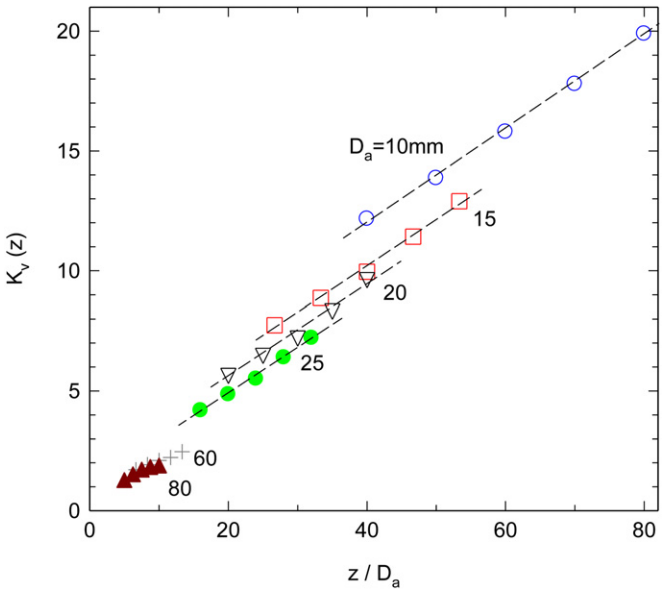

Fig. 17. Flue-gas recirculation rate (K_v) at different z for $D_f = 3$ mm, $S = 50.7$ mm, $T_a = 838$ K, $P = 18.5$ kW and $\phi = 0.85$.

air-fuel ratio (γ_s), equivalence ratio (ϕ), and initial temperature ratio (T_f/T_a). However, the geometric parameters appear to be more critical for controlling Z_J and K_v and thus the characteristics of diffusion MILD combustion.

Wünning & Wünning [2] provided a stability diagram for non-premixed MILD combustion of methane in a particular furnace system (Fig. 19). By relating the average furnace temperature T_{av} to K_v, three combustion regimes were identified and termed as Regions A, B and C (as indicated on the plot). Region A is characterized by stable conventional flames, Region B by an unstable transitional regime from conventional to MILD combustion, and Region C by the MILD regime. Wünning & Wünning [2] estimated K_v based only on the exhaust gas recirculated into reactants before their reaction takes place, excluding the recirculation of hot products into the reaction zone to improve combustion stability. This is similar to the present calculation of $K_v(Z_J)$. The present values of T_{av}, obtained by averaging the mean temperatures over the forward or positive velocity flow region, against $K_v(Z_J)$ are also shown on the same diagram of Fig. 19. Evidently, only the case for $D_a = 80$ mm falls in Region A and four in Region B while the rest ten are located in the stable MILD region, i.e., Region C. Our modelling results hence suggest that the detailed classification of Wünning & Wünning [2] should work only for their particular case.

The above suggestion coincides with the experimental result of Szegö et al. [7] obtained from a furnace of different configuration. These authors found that the lower limit for stable MILD combustion at a thermal input of 15 kW is $G_f/G_a \approx 0.006$, irrespective of firing NG or LPG. This was supported by their thermal field measurements. Therefore, they believed that the stability limits of $T_{av} - K_v$ depend on G_f/G_a. Eq. (9) suggests that $K_v(Z_J) \propto (G_f/G_a)^{1/4}$. In other words, if Eq. (9) is valid for diffusion combustion, the limit boundary of $T_v - K_v(Z_J)$ for the region "C" should depend on G_f/G_a. More specifically, it varies with burner geometric parameters

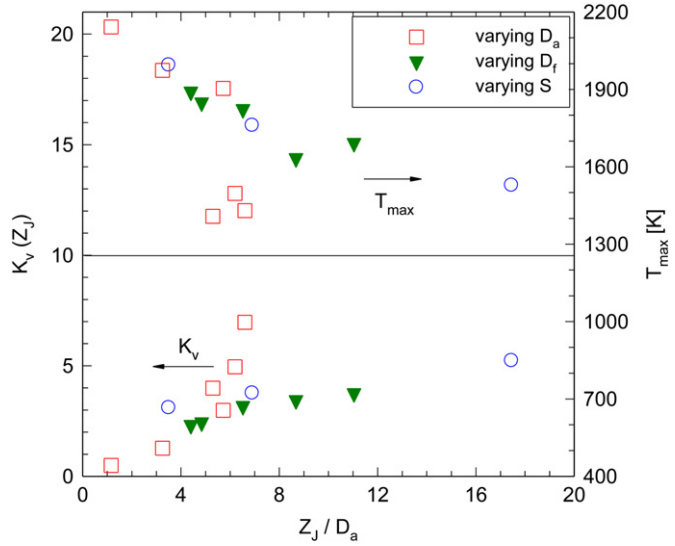

Fig. 16. Effects of Z_J on the flue-gas recirculation ratio $K_v(Z_J)$ and maximum mean temperature T_{max} for $T_a = 838$ K, $P = 18.5$ kW and $\phi = 0.85$.

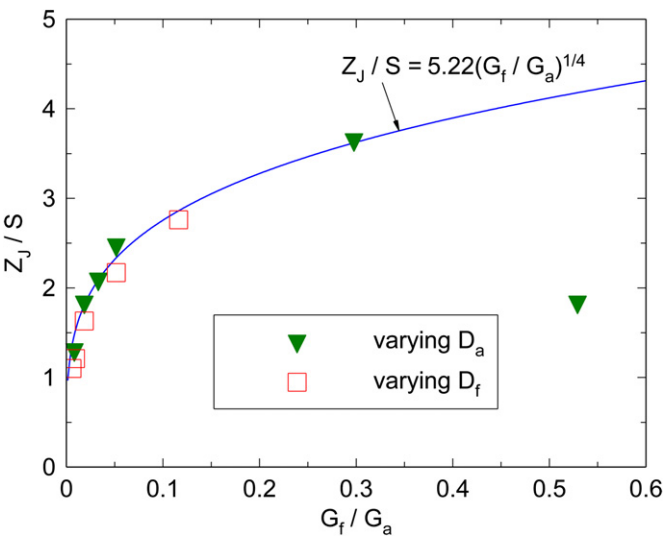

Fig. 18. Influence of the injection momentum ratio (G_f/G_a) on Z_J for $P = 18.5$ kW and $\phi = 0.85$.

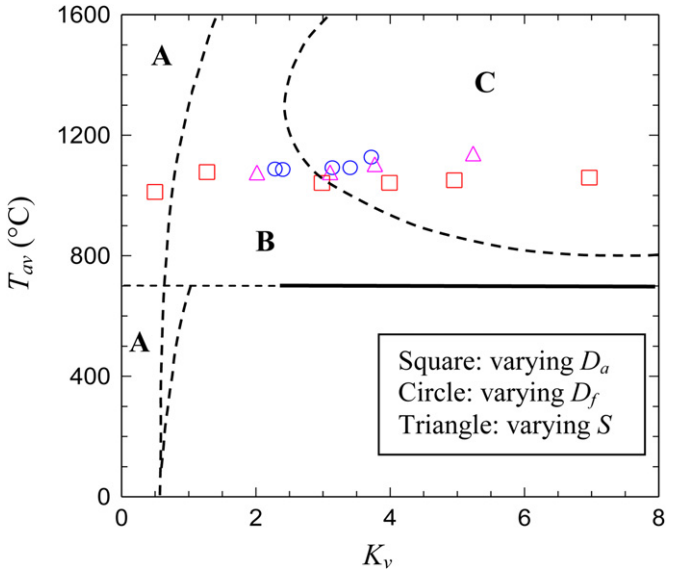

Fig. 19. Locally averaged mean temperature T_{av} against K_v at Z_J and the corresponding schematic diagram of stability limits of MILD combustion from Ref. [2].

(e.g., D_a, D_f, S), and also fuel type, air-fuel ratio and the inlet temperature. Szegö et al. [7] established stable MILD combustions in their furnace with $D_f = 2$ mm (higher G_f) but not $D_f = 3$ mm (lower G_f), because the fuel-jet penetration for the latter is too short to enable sufficient dilution of reactants for MILD combustion to occur. Hence, the stability limit for MILD combustion varies with different non-premixed combustor systems and also G_f/G_a.

6. Conclusions

A systematic study by the RANS-modelling has been carried out on the diffusion combustion of methane and air issuing from a parallel multi-jet burner at a laboratory-scale furnace. Different injection conditions have been considered that include the inlet separation between fuel and air jets (S), air nozzle diameter (D_a), fuel nozzle diameter (D_f), and air preheat temperature (T_a). For those cases measured by Rottier et al. [8], the modelling predicts reasonably well. It is thus believed that the present simulations should work qualitatively for other cases of investigation. Moreover, a fundamental analysis performed on the simulated results has led to several interesting relations.

The main conclusions drawn from the present study are summarized below:

(1) Two parameters are found important for investigating the diffusion MILD combustion of a multi-jet burner: i.e., the fuel-jet penetration distance Z_J and the relative rate of recirculation of exhaust gases occurring at the fuel-oxidant confluence point, $K_v(Z_J)$. Increasing either of the two generally yields higher dilution of reactants and is therefore beneficial for establishing the MILD combustion.

(2) In the burner/furnace system modelled, the fuel-jet penetration Z_J depend significantly on D_f, D_a and S. Increasing D_f and S can make fuel jets to delay their mixing with central air jet and hence the main reaction to occur in a lower-oxygen diluted zone. However, varying D_a appears to be the most effective way to control the magnitude of K_v and consequently the combustion performance and stability characteristics. By comparison, the properties of reactants have weaker effects on Z_J and $K_v(Z_J)$. These findings should also apply for other combustor systems using multi-jet burners.

(3) Based on the predicted data, the analytical approximations Eqs. (8) and (9) or Eqs. (10) and (11) appear to hold reasonably well for varying the initial fuel-air momentum ratio (G_f/G_a) or burner geometric parameters (S, D_a and D_f) in the diffusion combustion system modelled. Those approximations are believed to work also for other multi-jet burner systems if taking different values of C_e, C_1 and C_2. If they are indeed generally valid, even qualitatively, they should be significant and helpful for fundamental research and particularly technology development of the MILD combustion from a multi-jet burner system.

(4) The critical value of $K_v(Z_J)$ for the stable MILD combustion and thus the stability limits of different combustion modes vary with particular combustor, burner configurations, the injection momentum ratio G_f/G_a and reactant properties. Accordingly, the schematic diagram of Wünning & Wünning [2] obtained for a particular combustion system is not suggested to be used as a *quantitative* benchmark to assess whether or not the MILD combustion truly occurs in different combustors and/or under different reactant injection conditions.

Acknowledgements

The first author gratefully acknowledges the support from Foundation of State Key Laboratory of Coal Combustion of China. The present work is also funded by Major State Basic Research Development Program of China (973 Program) (No. 2011CB707301) and National Natural Science Foundation of China (No. 50936001). Here, we thank all the referees for providing insightful comments, the addressing of which has strengthened our paper significantly.

References

[1] Tsuji H, Gupta A, Katsuki M. High temperature air combustion: from energy conservation to pollution reduction. Florida: CRC Press; 2003.
[2] Wünning JA, Wünning JG. Flameless oxidation to reduce thermal no-formation. Progress in Energy and Combustion Science 1997;23(1):81–94.
[3] Cavaliere A, de Joannon M. Mild combustion. Progress in Energy and Combustion Science 2004;30(4):329–66.
[4] Weber R, Orsino S, Lallemant N, Verlaan A. Combustion of natural gas with high-temperature air and large quantities of flue gas. Proceedings of the Combustion Institute 2000;28:1315–21.
[5] Weber R, Smart JP, vd Kamp W. On the (MILD) combustion of gaseous, liquid, and solid fuels in high temperature preheated air. Proceedings of the Combustion Institute 2005;30:2623–9.
[6] Zhang H, Yue G, Lu J, Jia Z, Mao J, Fujimori T, et al. Development of high temperature air combustion technology in pulverized fossil fuel fired boilers. Proceedings of the Combustion Institute 2007;31(2):2779–85.
[7] Szego GG, Dally BB, Nathan GJ. Operational characteristics of a parallel jet MILD combustion burner system. Combustion and Flame 2009;156(2):429–38.
[8] Rottier C, Lacour C, Godard G, Taupin B, Porcheron L, Hauguel R, et al. On the effect of air temperature on mild flameless combustion regime of high temperature furnace. Proceedings of the European Combustion Meeting; 2009. Austria.
[9] Rottier C, Lacour C, Godard G, Taupin B, Boukhalfa AM, Honoré D, et al. Aerodynamic way to reach mild combustion regime in a laboratory-scale furnace. Proceedings of the European Combustion Meeting; 2007. Austria.
[10] Kumar S, Paul PJ, Mukunda HS. Studies on a new high-intensity low-emission burner. Proceedings of the Combustion Institute 2002;29:1131.
[11] Dally BB, Riesmeier E, Peters N. Effect of fuel mixture on moderate and intense low oxygen dilution combustion. Combustion and Flame 2004;137(4):418–31.
[12] Mi J, Li P, Dally BB, Craig RA. Influence of initial air-fuel premixing on MILD combustion in a recuperative fuenace. Energy & Fuels 2009;23(11):5349–56.
[13] Mi J, Li P, Zheng C. Numerical simulation of flameless premixed combustion with an Annular Nozzle in a recuperative furnace. Chinese Journal of Chemical Engineering 2010;18(1):10–7.
[14] Li P, Mi J, Dally BB, Craig RA, Wang F. Premixed MILD combustion from a single jet burner in a laboratory-scale furnace. Energy & Fuel; 2011. doi:10.1021/ef200208.

[15] Li P, Mi J. Influence of inlet dilution of reactants on premixed combustion in a recuperative furnace. Flow, Turbulence and Combustion 2011;85(4):1–22.
[16] Schaffel-Mancini N, Mancini M, Szlek A, Weber R. Novel conceptual design of a supercritical pulverized coal boiler utilizing high temperature air combustion (HTAC) technology. Energy 2010;35(7):2752–60.
[17] Masson E. Etude experimentale des champs dynamiques et scalaires de la combustion sans flame. The PhD thesis 2005: http://www.coria.fr/spip.php?article281&titre_mot=these.
[18] Fluent 6.3 Documentation. Fluent Inc.; 2007.
[19] Pope SB. Computationally efficient implementation of combustion chemistry using in situ adaptive tabulation. Combustion Theory and Modelling 1997; 1(1):41–63.
[20] Chui E, Raithby G. Computation of radiant heat transfer on a nonorthogonal mesh using the finite-volume method. Numerical Heat Transfer. Part B Fundamentals 1993;23(3):269–88.
[21] Turns S. An Introduction to combustion: concepts and applications. New York: McGraw-Hill; 1996.
[22] Pope SB. Turbulent Flows. Cambridge University Press; 2000.
[23] Ricou FP, Spalding DB. Measurement of local entrainment rate in the initial region of axisymmetric turbulent air jets. Journal of Fluid Mechanics 1961;11: 21–32.
[24] Grandmaison EW, Yimer I, Becker HA, Sobiesiak A. The strong-jet/weak-jet problem and aerodynamic modeling of the CGRI burner. Combustion and Flame 1998;114(3–4):381–96.